IAA-AAS-DyCoSS2-14 -15-01

FIRST-GUESS GENERATION OF SOLAR SAIL INTERPLANETARY HETEROCLINIC CONNECTIONS*

Giorgio Mingotti†, Jeannette Heiligers‡, and Colin McInnes§

This work deals with the generation of first-guess interplanetary trajectories connecting Libration Point Orbits (LPOs) belonging to different restricted three-body problems. With the Sun always as first primary, the Earth, Mars and Mercury are assumed as second primary, and their relative models are coupled together with the view of defining heteroclinic connections. On suitable Poincaré sections, solar sail sets are constructed to obtain transit conditions from LPOs of the departure dynamical system to LPOs of the arrival one. Constant attitude solar sails are investigated, assuming spacecraft with limited control capabilities. The preliminary propellant-free transfer trajectories are considered for a range of novel solar sail applications, including a continuous Earth–Mars communication link, an Earth–Mars cargo transport gateway and an opportunity for in-situ observations of Mercury.

INTRODUCTION

Solar sail technology is rapidly gaining momentum after recent successes, such as JAXA's mission IKAROS,[1] NASA's NanoSail-D2 mission, and after the development of NASA's Sunjammer mission.[2] By exploiting the radiation pressure generated by solar photons reflecting off a large, highly reflecting sail to produce a continuous thrust, solar sails are not constrained by propellant mass. Moreover, with the increase of the area-to-mass ratio, solar radiation pressure has a significant effect on the interplanetary transfer design process. Previous applications of solar sails have already been designed assuming the two-body problem, i.e. McInnes,[3] and the three-body problem, i.e. Baoyin.[4]

It is well-known that the three-body system generates five natural libration points, around which periodic orbits can be found (LPOs). By adding a solar sail to the dynamical model, the collinear libration points as well as the periodic orbits around them are displaced Sunward along the Sun-sail line. Therefore, natural L_1- and L_2-orbits will therefore shift away and towards the secondary body, respectively, allowing for additional interesting science.[5] While heteroclinic connections between sail displaced LPOs of the same restricted three-body problem have already been investigated,[4] interplanetary solar sail transfers between different three-body systems have never been addressed.

†Research Associate, Advanced Space Concepts Laboratory, Department of Mechanical & Aerospace Engineering, University of Strathclyde, 75 Montrose Street, G1 1XJ Glasgow, United Kingdom. e-mail: giorgio.mingotti@strath.ac.uk

‡Research Associate, Advanced Space Concepts Laboratory, Department of Mechanical & Aerospace Engineering, University of Strathclyde, 75 Montrose Street, G1 1XJ Glasgow, United Kingdom. e-mail: jeannette.heiligers@strath.ac.uk

§Professor, Advanced Space Concepts Laboratory, Department of Mechanical & Aerospace Engineering, University of Strathclyde, 75 Montrose Street, G1 1XJ Glasgow, United Kingdom. e-mail: colin.mcinnes@strath.ac.uk

Such transfers are of importance for generating efficient trajectories with a (near) constant sail attitude, with applications to small satellite science missions, or even future round-trip cargo missions.

The aim of this paper is to describe the first-guess generation process - based on a few design variables - of solar sail trajectories for two different applicative scenarios. Both the connections of a natural Earth L_2-orbit with a natural Mars L_1-orbit and of a natural Earth L_1-orbit with a natural Mercury L_2-orbit are investigated, thereby building on the concept named "patched restricted three-body problems approximation".[6] In this approach, intersections in configuration space of the invariant manifolds of the two restricted three-body problems are searched for. For example, the unstable manifold of a northern Halo L_2-orbit in the Sun–Earth problem is considered in combination with the stable manifold of a northern Halo L_1-orbit in the Sun–Mars problem. If these intersect in the configuration space, an Earth–Mars low-energy transfer, with at most one deep-space manoeuvre, exists. Unfortunately, no intersection exists among ballistic manifolds of inner planets.[7]

Special *dedicated sets* are then introduced to exploit the combined use of solar radiation pressure with invariant manifold trajectories, aiming at defining feasible first guess solutions. This approach enables a radically new class of missions, whose solutions are not obtainable neither through the patched-conics method nor through the classic invariant manifolds technique. The key idea is to replace invariant manifolds with *solar sail sets*, and to manipulate the latter in the same way the manifolds are used to design space transfers.[8] By including a solar sail acceleration and fixing the attitude of the solar sail with respect to the Sun-sail line, intersections between restricted three-body models can be found on suitable Poincaré sections, also for the inner planets. Alongside the exploitation of the n-body problems' intrinsic dynamics, the propellant-free feature of solar sails is used in order to define efficient trajectories.

The paper is organized as follows. In the first section some background notions on the circular restricted three-body problem, its periodic orbits and invariant manifold structure are given. Then, the second section introduces solar radiation pressure into the restricted three-body problem and defines the special dedicated sets. In the third section the first guess design technique is formulated: the solar sail interplanetary heteroclinic connections are generated. The preliminary transfer trajectories are discussed in the fourth section and conclusive remarks are given in the last one.

DYNAMICAL MODEL

In this section, the dynamical system investigated in this work is described, i.e. the three-dimensional Circular Restricted Three-Body Problem (CRTBP), with its periodic orbits and invariant manifold structure. The dynamics described in the following holds for the Sun–Earth (SE), the Sun–Mars (SM) and the Sun–Mercury (SM) problem, respectively.

The Three-Dimensional Circular Restricted Three-Body Problem

The motion of the spacecraft, P_3, of mass m_3, is studied in the gravitational field generated by two primaries, P_1, P_2, of masses m_1, m_2, respectively, assumed to move in circular motion about their common center of mass (see Fig. 1(a)). It is assumed that P_3 moves under the non-dimensional equations[9]

$$\ddot{x} - 2\dot{y} = \frac{\partial \Omega}{\partial x}, \qquad \ddot{y} + 2\dot{x} = \frac{\partial \Omega}{\partial y}, \qquad \ddot{z} = \frac{\partial \Omega}{\partial z}, \tag{1}$$

where the auxiliary function is

$$\Omega(x, y, z, \mu) = \frac{1}{2}(x^2 + y^2) + \frac{1-\mu}{r_1} + \frac{\mu}{r_2} + \frac{1}{2}\mu(1-\mu), \tag{2}$$

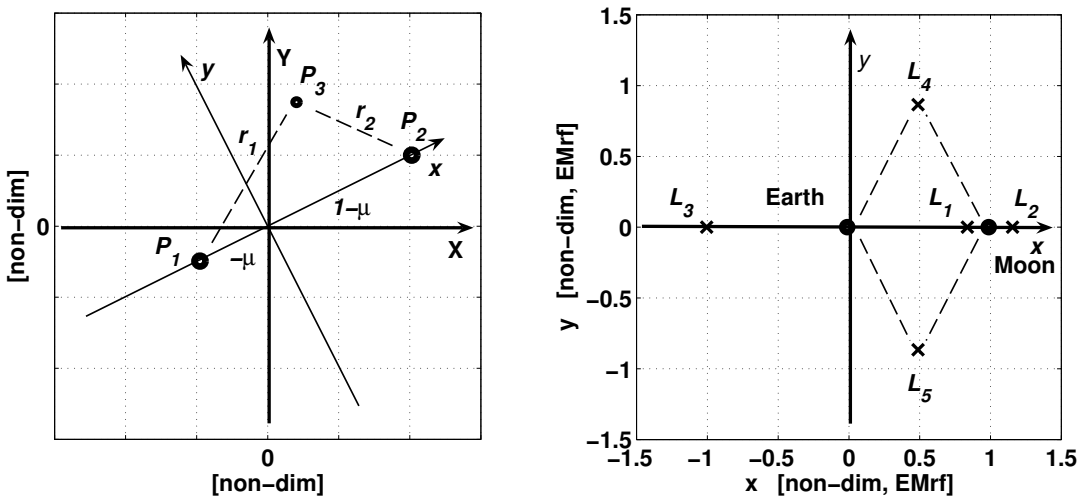

(a) Circular restricted three-body problem.

(b) Libration point location.

Figure 1. Circular restricted three-body problem geometry and libration point location.

and $\mu = m_2/(m_1 + m_2)$ is the mass parameter of the three-body problem. Eqs. 1 are written in a barycentric rotating frame with non-dimensional units: the angular velocity of P_1, P_2, their distance, and the sum of their masses are all set to the unit value. Thus, P_1, P_2 have scaled masses $1 - \mu$, μ, and are located at $(-\mu, 0)$, $(1 - \mu, 0)$, respectively. The distances in Eq. 2 are therefore

$$r_1^2 = (x + \mu)^2 + y^2 + z^2, \qquad r_2^2 = (x + \mu - 1)^2 + y^2 + z^2. \tag{3}$$

For fixed μ, the energy of P_3 is represented by the Jacobi integral which reads

$$\mathcal{J}(x, y, z, \dot{x}, \dot{y}, \dot{z}) = 2\Omega(x, y, z) - (\dot{x}^2 + \dot{y}^2 + \dot{z}^2), \tag{4}$$

and, for a given energy $\mathcal{C}$, it defines a three-dimensional manifold

$$\mathcal{M}(\mathcal{C}) = \{(x, y, z, \dot{x}, \dot{y}, \dot{z}) \in \mathbb{R}^6 \,|\, \mathcal{J}(x, y, z, \dot{x}, \dot{y}, \dot{z}) - \mathcal{C} = 0\}. \tag{5}$$

The projection of $\mathcal{M}$ on the configuration space (x, y) defines the Hill's curves bounding the allowed and forbidden regions of motion associated with prescribed values of $\mathcal{C}$. The aforementioned three-dimensional manifold of the states of motion has singular points which are also equilibrium points for the dynamical system. The CRTBP is used to model the third body motion in the Sun–Earth system, whose mass parameter is $\mu = 3.003460 \times 10^{-6}$ (therefore not including the Moon mass), in the Sun–Mars system, whose mass parameter is $\mu = 3.226835 \times 10^{-7}$, and in the Sun–Mercury system, whose mass parameter is $\mu = 1.660148 \times 10^{-7}$.[9]

The CRTBP has five well-known equilibrium points, L_j, whose energy is $\mathcal{C}j$, $j = 1, \ldots, 5$. They are classified as *collinear* (L_1, L_2, L_3), which belong to the x-axis of the rotating reference system, and as *equilateral* (see Fig. 1(b)). The latter form two equilateral triangles, symmetric with respect to the x-axis, with the two primaries as vertexes.[10–12]

Table 1. Departure and arrival LPOs for both the Earth-to-Mars and the Earth-to-Mercury applicative scenarios. NH stands for northern Halo orbit and SH stands for southern Halo orbit. A_z is the out-of-plane amplitude, $\mathcal{C}$ is the Jacobi constant and P_O is the period of the selected departure and arrival orbits.

Departure Orbit	A_z [km]	$\mathcal{C}$ [−, SErf]	P_O [−, SErf]	Arrival Orbit	A_z [km]	$\mathcal{C}$ [−, SMrf]	P_O [−, SMrf]
Ea NH-L2	650×10^3	3.0006797	3.0741	Ma NH-L1	350×10^3	3.0001705	3.0602
Ea NH-L1	650×10^3	3.0006874	3.0388	Me SH-L2	150×10^3	3.0000957	3.0555

Libration Point Periodic Orbits

Concerning the CRTBP, around the three collinear equilibrium points and associated with their center-like behavior, there are periodic and quasi-periodic orbits. Recalling the conservative property of Hamiltonian systems, periodic orbits can be grouped in families and they are function of just one scalar: the amplitude A of the orbit. In detail, the orbits related to the linear oscillators of the linearized problem belong to the Lyapunov family, planar and vertical.

There is an analytic solution of the latter, associated with the linearized problem and thus characterized by infinitesimal dimensions. Space mission design usually involves Lyapunov orbits with prescribed wider amplitude and governed by the complete dynamics of the problem. The computation of these orbits is obtained through a numerical approach, based on *perturbation* techniques, in order to correct the analytic initial estimates, and on *continuation* techniques, in order to expand the infinitesimal orbits. Other interesting solutions are the two-dimensional tori, associated with the Lissajous orbits arising from the product of the two linear oscillators.

It is well known from theory, that if the phase space of a dynamical system changes substantially varying the value of a certain parameter, this behavior is known as *bifurcation* phenomenon. In the CRTBP framework, the planar Lyapunov orbits defined with the amplitude A as unique parameter, according to the bifurcation effect, give origin to a family of three-dimensional orbits with a different period and with a modified relative invariant manifold structure.

Moreover, once the *out-of-plane* A_z amplitude overcomes a limit value $\bar{A}_z$, the frequency of the *in-plane* oscillatory motion achieves the value of the frequency of the one out of the plane, and three-dimensional halo orbits emerge.[13] The lack of an analytic solution in the CRTBP, the significant nonlinearity of the problem as well as the strong dependence on variations of initial conditions, imply that the determination of such orbits is not trivial: their computation is possible starting from a semi-analytic formulation, according to the systematic approach proposed by Richardson,[14,15] and then following approximations based on differential corrections.

In this paper, two different types of libration point orbits are investigated: three-dimensional (x, z)-plane symmetric northern Halo (with the maximum out-of-plane displacement $z > 0$) and three-dimensional (x, z)-plane symmetric southern Halo (with the maximum out-of-plane displacement $z < 0$).

Invariant Manifold Structure

In the CRTBP framework, a set can be said to be invariant if any orbit that originates from itself is bounded within limits during the time evolution of the dynamics: namely, an invariant mani-

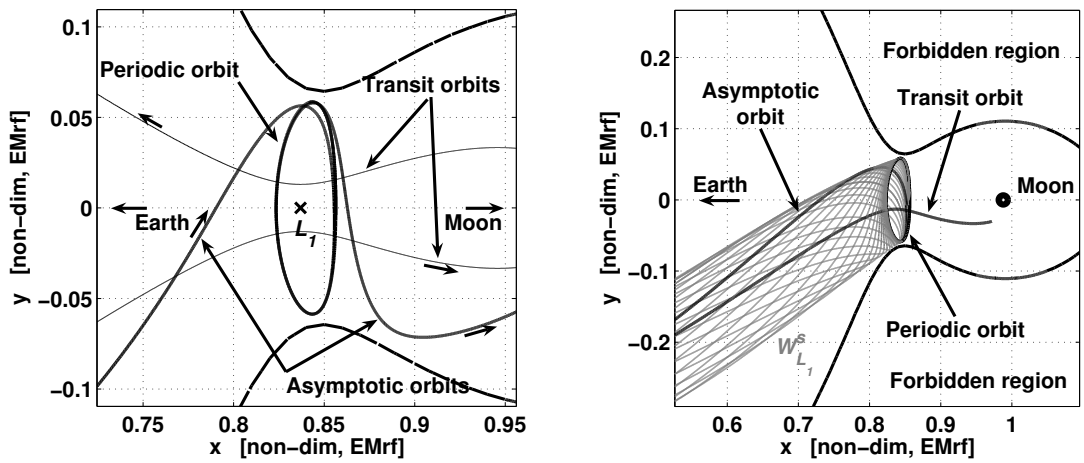

(a) Orbital motion around the libration point L_1 in the Earth–Moon system.

(b) Invariant manifold structure associated to a LPO around L_1 in the Earth–Moon system.

Figure 2. Orbital motion and invariant manifold structure around the libration point L_1.

fold can be viewed as a combination of orbits that form a surface. In detail, equilibrium points, periodic orbits as well as the Jacobi integral expressed in Eq. 4, all represent invariant manifolds, zero-dimensional, one-dimensional and five-dimensional, respectively. The motion that starts from any of those manifolds is bounded in the same subspace of its origin, under the flow of the dynamical system. From the perspective of space mission analysis, one-dimensional stable and unstable manifolds V_{L_j} related to the fixed points, as well as the two-dimensional ones W_{L_j} associated with the periodic orbits around the same points, for $j = 1, 2$, are of great interest.

Invariant manifolds associated with LPOs are appealing for space mission design (see Fig. 2). They are classified in stable $W^s_{L_j}$, for $j = 1, 2$, if the third body - from an initial condition belonging to the surface itself - asymptotically moves to the periodic orbit; moreover, if a spacecraft from an initial condition on $W^u_{L_j}$, for $j = 1, 2$, moves indefinitely away from a periodic orbit, that manifold is said to be unstable. Such surfaces in the configuration space have a *tube*-like structure and they play a role of *separatrices*[16] of the motion: trajectories inside these subspaces are transit orbits that allow the third body to move from one primary to the other, while those outside these subspaces are non-transit orbits.

As far as it concerns the CRTBP, in order to investigate the hyperbolic-like behavior of periodic orbits around libration points, the classic approach is based on the Floquet theory that studies the linear approximation of the flow mapping around a periodic orbit.[17] Thus, once the state transition matrix associated with a periodic orbit is obtained, the *monodromy* matrix $\mathbf{M}$, the manifolds are computed by propagating the flow along the directions corresponding to the Floquet multipliers of that orbit. In particular, if $\mathbf{y}$ is a point belonging to the periodic orbit, the monodromy matrix represents the first-order approximation for the mapping of a point $\mathbf{y}_k$, considered in a small neighborhood, through

$$\mathbf{y} \mapsto \mathbf{y}_k + \mathbf{M}(\mathbf{y} - \mathbf{y}_k). \tag{6}$$

In detail, it is possible to construct the two-dimensional stable manifold $W^s_{L_j}$, for $j = 1, 2$, as the connection of all the one-dimensional stable manifolds associated with each q point of the periodic

orbit, named $\mathbf{y}^q$

$$\mathbf{y}^q_{k,s} = \mathbf{y}^q \pm \varepsilon \mathbf{v}^q_s. \tag{7}$$

In the same way, the two-dimensional unstable manifold $W^u_{L_j}$, for $j = 1, 2$, is formulated as

$$\mathbf{y}^q_{k,u} = \mathbf{y}^q \pm \varepsilon \mathbf{v}^q_u, \tag{8}$$

where $\varepsilon = 1.0 \times 10^{-6}$ is a scalar parameter that represents the *magnitude* of the shift along the stable $\mathbf{v}^q_s$ and unstable $\mathbf{v}^q_u$ normalized eigenvector of the monodromy matrix $\mathbf{M}$ evaluated at the fixed point $\mathbf{y}^q$, respectively.[18]

The symbol $\pm$ denotes the existence of two branches for each manifold. Considering the fixed point L_1 of Sun–Earth system, the branch associated with the symbol $-$ is the branch of the manifold originating from the L_1-region and moving, internally, in the direction of the Sun ($W^{s,I}_{L_1}$, $W^{u,I}_{L_1}$). On the other hand, the branch of the manifold related to the symbol $+$ is the one departing from the L_2-region and moving, externally, away from the Earth ($W^{s,E}_{L_2}$, $W^{u,E}_{L_2}$).

Finally, it is possible to flow the previous initial conditions, obtained through the linear analysis, under the complete nonlinear differential system of Eqs. 1. This is valid thanks to the property that the stable and unstable manifolds associated with periodic orbits are locally tangent at the origin to the subspace of the eigenvectors of the monodromy matrix.[9–11]

SOLAR RADIATION PRESSURE AND DEDICATED SETS

In this section, the perturbed circular restricted three-body problem by a prescribed control law and special *dedicated sets* are introduced. As a direct consequence, the *solar sail sets* associated to the departure and arrival periodic orbits are described. The formulation holds for the Sun–Earth, the Sun–Mars and the Sun–Mercury system, respectively.

The Perturbed, Three-Dimensional Circular Restricted Three-Body Problem

To model the motion of a massless particle P_3 under both the gravitational attractions of P_1, P_2, and solar radiation pressure, the perturbed CRTBP is introduced:[19]

$$\ddot{x} - 2\dot{y} = \frac{\partial \Omega}{\partial x} + a_s s_x, \qquad \ddot{y} + 2\dot{x} = \frac{\partial \Omega}{\partial y} + a_s s_y, \qquad \ddot{z} = \frac{\partial \Omega}{\partial z} + a_s s_z, \tag{9}$$

where $\hat{\mathbf{s}} = (s_x, s_y, s_z)^\top$ is the normalized acceleration direction due to the effect of solar radiation pressure on the sail surface and, considering an ideal sail, it is aligned with its normal component $\hat{\mathbf{n}}$, i.e. $\hat{\mathbf{s}} \equiv \hat{\mathbf{n}}$. The magnitude of this acceleration is

$$a_s = \beta \frac{1-\mu}{r_1^2} (\hat{\mathbf{s}} \cdot \hat{\mathbf{r}}_1)^2, \tag{10}$$

where β is the lightness number of the sail and $\mathbf{r}_1 = (x + \mu, y, z)^\top$ is the Sun-sail line vector. Moreover, the angle $\alpha = \cos^{-1}(\hat{\mathbf{s}} \cdot \hat{\mathbf{r}}_1)$ is known as the *cone angle* (see Fig. 3(a)).

Assuming that the attitude of the sail is controllable, solar radiation pressure rather than a passive perturbation becomes a way to control the orbital dynamics of the spacecraft. In addition to the cone angle, another angle is introduced to univocally define the attitude of the solar sail: the *clock angle* δ (see Fig. 3(b)), that is the angle measured clockwise around $\hat{\mathbf{r}}_1$, starting from the vertical plane, of

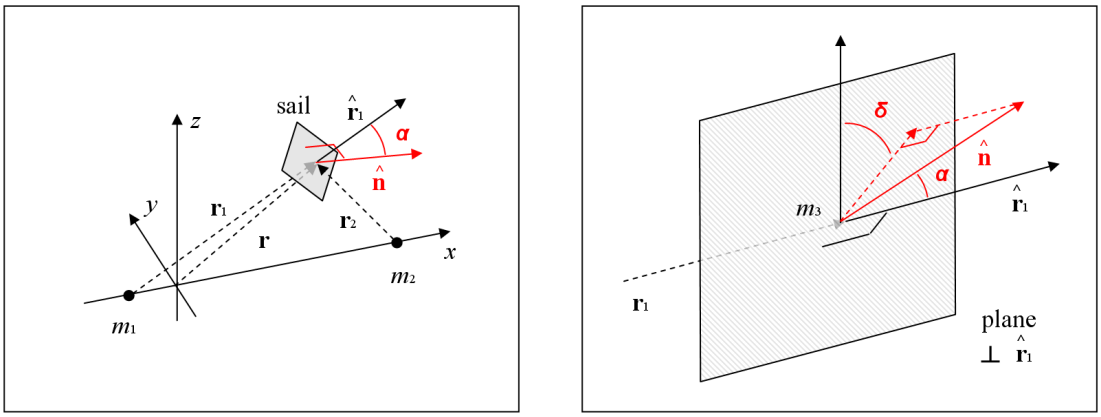

(a) Solar sail geometry: the cone angle α.

(b) Solar sail geometry: the clock angle δ.

Figure 3. Solar sail geometry in the circular restricted three-body problem: the cone angle α and the clock angle δ.

the component of $\hat{\mathbf{n}}$ perpendicular to $\hat{\mathbf{r}}_1$ (recalling that for an ideal sail, i.e. $\hat{\mathbf{s}} \equiv \hat{\mathbf{n}}$). In order to build first guess solutions, the control direction $\hat{\mathbf{s}}(t) = (s_x(t), s_y(t), s_z(t))^\top$, with $t \in [t_i, t_f]$, in Eqs. 9 is a-priori imposed, giving, at this stage, to the control law $\mathbf{R}(t) = a_s\hat{\mathbf{s}}(t)$ a prescribed shape. In detail, the profile over time of the cone angle $\alpha(t)$ and the clock angle $\delta(t)$ is assigned. Dedicated solar sail sets can be defined under this assumption.

Definition of Solar Sail Dedicated Sets

Let $\mathbf{y}_i$ be a vector representing a generic initial state, $\mathbf{y}_i = (x_i, y_i, z_i, \dot{x}_i, \dot{y}_i, \dot{z}_i)$; then let the flow of system of Eqs. 9 be $\phi_{\mathbf{R}}(\mathbf{y}_i, t_i; t)$ at time t starting from $(\mathbf{y}_i, t_i)$ and considering the control law, based on the exploitation of solar radiation pressure, $\mathbf{R}(\alpha, \delta, t) = a_s\hat{\mathbf{s}}(t)$, $t \in [t_i, t_f]$.

With this notation, it is possible to define the generic point of a solar sail trajectory through

$$\mathbf{y}(t) = \phi_{\overline{\mathbf{R}}}(\mathbf{y}_i, t_i; \alpha, \delta, t), \tag{11}$$

where $\overline{\mathbf{R}}$ is the control vector assuming a fixed attitude solar sail with respect to the Sun-sail line, i.e. with constant cone angle α and constant clock angle δ. Solar sail acceleration magnitude is then computed via Eq. 10.

Let $P(\epsilon)$ and $Q(\theta)$ be two surfaces of section perpendicular to the (x, y)-plane: the first one is perpendicular to the x-axis and is located at a ϵ distance (along the x-axis) from the rotating frame origin, while the second one forms an angle θ with the x-axis.

The solar sail orbit, for chosen values of ϵ and θ, is

$$\gamma_{\overline{\mathbf{R}}}(\mathbf{y}_i, \alpha, \delta, \tau, \epsilon, \theta) = \left\{\phi_{\overline{\mathbf{R}}}(\mathbf{y}_i, t_i; \alpha, \delta, \tau) \,|\, 0 \leq \tau \leq t_Q - t_P\right\}, \tag{12}$$

where the dependence on the initial state $\mathbf{y}_i$ is kept. In Eq. 12, τ is the duration of the solar sail contribution, whereas t_P, t_Q are the time at which the orbit intersects $P(\epsilon)$ (for the first time) and $Q(\theta)$, respectively. Assuming the orbit crosses section $P(\epsilon)$ before $Q(\theta)$, i.e. $t_P \leq t_Q$, the solar sail is active (i.e. $\hat{\mathbf{s}}$ in not orthogonal to $\hat{\mathbf{r}}_1$) only in the $t \in [t_P, t_Q]$ time interval.

The solar sail dedicated set is a collection of solar sail orbits (all computed with the same guidance law $\overline{\mathbf{R}}(\alpha, \delta)$ till they reach the surface $Q(\theta)$:

$$S_{\overline{\mathbf{R}}}(\alpha, \delta, \tau, \epsilon, \theta) = \bigcup_{\mathbf{y}_i \in \mathcal{Y}} \gamma_{\overline{\mathbf{R}}}(\mathbf{y}_i, \alpha, \delta, \tau, \epsilon, \theta). \tag{13}$$

According to the definition in Eq. 13, the solar sail dedicated set is made up by orbits that reach $Q(\theta)$ at different times, although all orbits have the same solar sail constant attitude. The cut, in the phase space, of the solar sail dedicate set with the surface $Q(\theta)$ is named $\partial S_{\overline{\mathbf{R}}}(\alpha, \delta, \tau, \epsilon, \theta)$.

The solar sail dedicated set in Eq. 13 is associated to a generic domain of admissible initial conditions $\mathcal{Y}$; it will be shown in the following how $\mathcal{Y}$ can be defined for solar sail departure and arrival sets, from and to selected periodic orbits, respectively. Thanks to the definition of $S_{\overline{\mathbf{R}}}(\alpha, \delta, \tau, \epsilon, \theta)$, the solar sail acceleration can be incorporated in a three-body frame using the same methodology developed for the invariant manifolds. More specifically, invariant manifolds and solar sail trajectories are replaced by dedicated sets which are manipulated to find connection points on suitable surfaces of section. The idea is to reproduce the role acted by invariant manifolds.

Solar Sail Departure Sets

In this paper, the initial orbits are LPOs in the Sun–Earth CRTBP, belonging to the northern and southern Halo families. The orbital amplitude (A) or the energy level of the final periodic orbits ($\mathcal{C}$) are assumed as given by mission requirements (see Tab. 1).

In detail, the initial state of the transfers, $\mathbf{y}_i$, can be any point that belongs to the selected LPOs, slightly perturbed along the direction of the unstable eigenvector of the periodic orbit monodromy matrix. Therefore, the initial point is the generic departing point

$$\mathbf{y}_i = \mathbf{y}_i(\tau_O^D) = \phi(\mathbf{y}_O^D, 0; \tau_O^D) \pm \varepsilon \mathbf{v}_u, \tag{14}$$

and is found by flowing the initial nominal point $\mathbf{y}_O^D$ for a time $\tau_O^D \leq P_O^D$, being P_O the initial orbit period and adding the small perturbation $\varepsilon = 1.0 \times 10^{-6}$ along the unstable eigenvector $\mathbf{v}_s$ (the $\pm$ ambiguity is solved by choosing $+$ to generate the exterior branch of the L_2-region manifold for the Earth-to-Mars mission scenario and $-$ to generate the interior branch of the L_1-region manifold for the Earth-to-Mercury mission scenario). The subscript $(\cdot)_O$ stands for the specific departure LPO selected.

The domain of admissible initial states is then written as follows

$$\mathcal{Y}^D = \{\mathbf{y}_i(\tau_O^D) | \tau_O^D \in [0, P_O^D]\}, \tag{15}$$

and the periodic orbit solar sail departure set, for some $\alpha_D \neq 90$ deg, $\tau_D > 0$, is given by the forward integration

$$D_{\overline{\mathbf{R}}}^{\mathrm{O}}(\alpha_D, \delta_D, \tau_D, \epsilon_D, \theta_D) = \bigcup_{\mathbf{y}_i \in \mathcal{Y}^D} \gamma_{\overline{\mathbf{R}}}(\mathbf{y}_i, \alpha_D, \delta_D, \tau_D, \epsilon_D, \theta_D). \tag{16}$$

The superscript $(\cdot)^{\mathrm{O}}$ stands for the specific departure LPO selected.

When the cone angle $\alpha_D = 90$ deg, there is no solar sail acceleration and the classic unstable manifolds of the relative LPOs are found as $W_{\overline{\mathbf{0}}}^{\mathrm{O}}(90, \delta_D, 0, \epsilon_D, \theta_D)$, directly following from Eq. 16. The cut, in the phase space, of the periodic orbit solar sail departure set with the surface $Q_D(\theta_D)$ is named $\partial D_{\overline{\mathbf{R}}}^{\mathrm{O}}(\alpha_D, \delta_D, \tau_D, \epsilon_D, \theta_D)$, while the cut of the set describing the classic unstable manifold trajectories is named $\partial W_{\overline{\mathbf{0}}}^{\mathrm{O}}(90, \delta_D, 0, \epsilon_D, \theta_D)$.

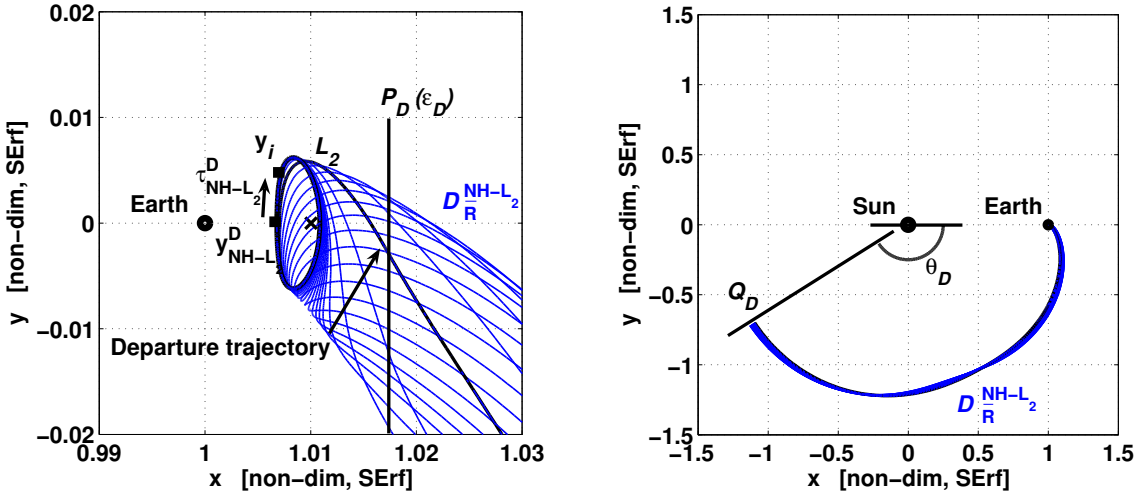

(a) Earth-to-Mars scenario: departure libration point orbit.

(b) Earth-to-Mars scenario: departure solar sail set.

Figure 4. Earth-to-Mars scenario: departure conditions and design variables. The blue solid lines represent the departure solar sail set $D_{\overline{\mathbf{R}}}^{\mathbf{NH\text{-}L_2}}(\alpha, \delta, \tau_D, \epsilon_D, \theta_D)$.

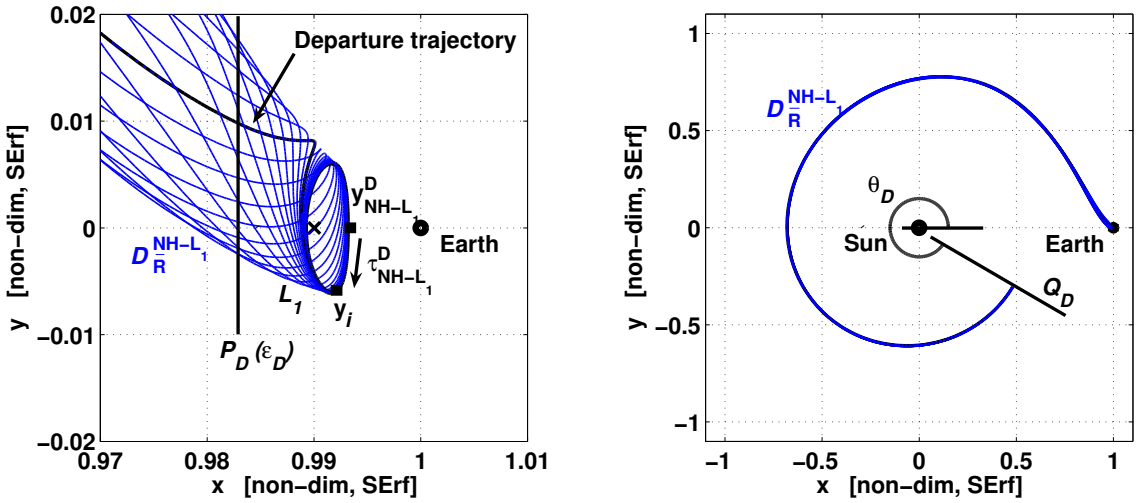

(a) Earth-to-Mercury scenario: departure libration point orbit.

(b) Earth-to-Mercury scenario: departure solar sail set.

Figure 5. Earth-to-Mercury scenario: departure conditions and design variables. The blue solid lines represent the departure solar sail set $D_{\overline{\mathbf{R}}}^{\mathbf{NH\text{-}L_1}}(\alpha, \delta, \tau_D, \epsilon_D, \theta_D)$.

Solar Sail Arrival Sets

As far as it concerns the target orbits, they are periodic orbits in the Sun–Mars and the Sun–Mercury CRTBPs, belonging to the northern and southern Halo families. The orbital amplitude (A) or the energy level of the final periodic orbits ($\mathcal{C}$) are assumed as given by mission requirements (see Tab. 1).

In detail, the final state of the transfers, $\mathbf{y}_f$, can be any point that belongs to the selected LPOs,

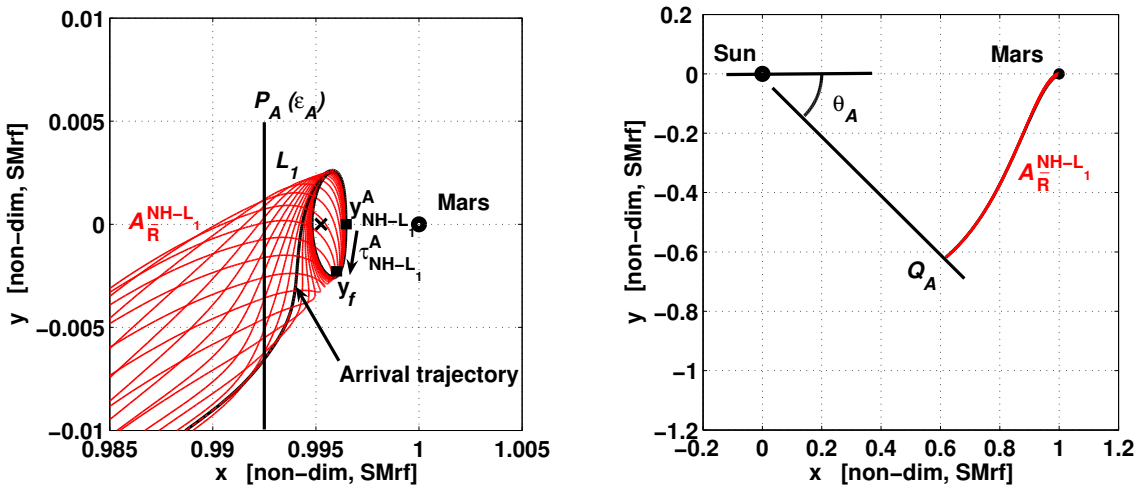

(a) Earth-to-Mars scenario: arrival libration point orbit.

(b) Earth-to-Mars scenario: arrival solar sail set.

Figure 6. Earth-to-Mars scenario: arrival conditions and design variables. The red solid lines represent the arrival solar sail set $A_{\mathbf{R}}^{\mathbf{NH\text{-}L_1}}(\alpha, \delta, -\tau_A, \epsilon_A, \theta_A)$.

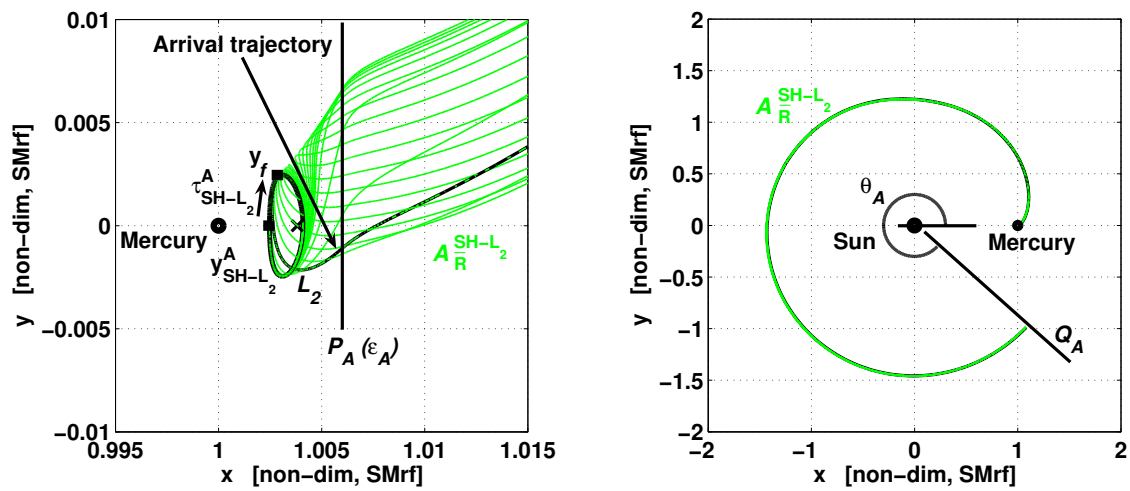

(a) Earth-to-Mercury scenario: arrival libration point orbit.

(b) Earth-to-Mercury scenario: arrival solar sail set.

Figure 7. Earth-to-Mercury scenario: arrival conditions and design variables. The green solid lines represent the arrival solar sail set $A_{\mathbf{R}}^{\mathbf{SH\text{-}L_2}}(\alpha, \delta, -\tau_A, \epsilon_A, \theta_A)$.

slightly perturbed along the direction of the stable eigenvector of the periodic orbit monodromy matrix. Therefore, the final point is the generic insertion point

$$\mathbf{y}_f = \mathbf{y}_f(\tau_O^A) = \phi(\mathbf{y}_O^A, 0; \tau_O^A) \pm \varepsilon \mathbf{v}_s, \tag{17}$$

and is found by flowing the initial nominal point $\mathbf{y}_O^A$ for a time $\tau_O^A \leq P_O^A$, being P_O^A the final orbit period and adding the small perturbation $\varepsilon = 1.0 \times 10^{-6}$ along the stable eigenvector $\mathbf{v}_s$ (the $\pm$ ambiguity is solved by choosing $+$ to generate the exterior branch of the L_2-region manifold for the Earth-to-Mercury mission scenario and $-$ to generate the interior branch of the L_1-region

manifold for the Earth-to-Mars mission scenario). The subscript $(\cdot)_O$ stands for the specific arrival LPO selected.

The domain of admissible final states is then written as follows

$$\mathcal{Y}^A = \{\mathbf{y}_f^A(\tau_O) | \tau_O^A \in [0, P_O^A]\}, \tag{18}$$

and the periodic orbit solar sail arrival set, for some $\alpha_A \neq 90$ deg, $\tau_A > 0$, is given by the backward integration

$$A_{\overline{\mathbf{R}}}^{\mathrm{O}}(\alpha_A, \delta_A, -\tau_A, \epsilon_A, \theta_A) = \bigcup_{\mathbf{y}_f \in \mathcal{Y}^A} \gamma_{\overline{\mathbf{R}}}(\mathbf{y}_f, \alpha_A, \delta_A, -\tau_A, \epsilon_A, \theta_A). \tag{19}$$

The superscript $(\cdot)^{\mathrm{O}}$ stands for the specific arrival LPO selected.

When the cone angle $\alpha_A = 90$ deg, there is no solar sail acceleration and the classic stable manifolds of the relative LPOs are found as $W_{\overline{\mathbf{0}}}^{\mathrm{O}}(90, \delta_A, -0, \epsilon_A, \theta_A)$, directly following from Eq. 19. The cut, in the phase space, of the periodic orbit solar sail arrival set with the surface $Q_A(\theta_A)$ is named $\partial A_{\overline{\mathbf{R}}}^{\mathrm{O}}(\alpha_A, \delta_A, -\tau_A, \epsilon_A, \theta_A)$, while the cut of the set describing the classic stable manifold trajectories is named $\partial W_{\overline{\mathbf{0}}}^{\mathrm{O}}(90, \delta_A, -0, \epsilon_A, \theta_A)$.

TRANSFER DESIGN TECHNIQUE

In this section, the transfer mechanism to design solar sail heteroclinic connections is described. The key idea to generate first guess solutions is to replace invariant manifolds with solar sail dedicated sets, and to manipulate the latter in the same way the manifolds are used to design space transfers.[8] With the inclusion of the solar sail acceleration and keeping the attitude of the solar sail constant - throughout the complete transfer - with respect to the Sun-sail line, intersections between restricted three-body models can be found on suitable Poincaré sections, also for the Earth-to-Mars and the Earth-to-Mercury cases. Therefore, the propellant-free feature of solar sails is combined with the exploitation of the n-body problems' intrinsic dynamics with a view of generating efficient trajectories. In detail, the technique to build first guesses, with the introduction of a few design variables, is split into basic phases as follows.

(i) The initial state of the transfers can be any point that belongs to the selected departure LPOs in the Sun–Earth CRTBP (around L_2 for the Earth-to-Mars mission scenario, around L_1 for the Earth-to-Mercury mission scenario), slightly perturbed along the direction of the unstable eigenvector of the periodic orbit monodromy matrix, as stated by Eq. 14.

(ii) The initial state is then propagated forward until it intersects a suitable Poincaré surface of section $Q_D(\theta_D)$, perpendicular to the (x, y)-plane and forming an angle θ_D with the x-axis, after crossing a previous section $P_D(\epsilon_D)$; as already described, the solar sail control is allowed (i.e. the sail is active) only between these two surfaces. If the trajectory is purely ballistic, then it moves along the unstable manifold of the selected LPO, i.e. on $W_{\overline{\mathbf{0}}}^{\mathrm{O}}(90, \delta_D, 0, \epsilon_D, \theta_D)$, otherwise, if solar radiation pressure is actively exploited, then it moves along the solar sail periodic orbit departure set $D_{\overline{\mathbf{R}}}^{\mathrm{O}}(\alpha_D, \delta_D, \tau_D, \epsilon_D, \theta_D)$.

(iii) The final state of the transfers can be any point that belongs to the selected arrival LPOs (around L_1 in the Sun–Mars CRTBP for the Earth-to-Mars mission scenario, around L_2 in the Sun–Mercury CRTBP for the Earth-to-Mercury mission scenario), slightly perturbed along the direction of the stable eigenvector of the periodic orbit monodromy matrix, as stated by Eq. 17.

Table 2. Values of the design variables for the generation of interplanetary (Earth-to-Mars, Earth-to-Mercury) heteroclinic first guess connections.

Applicative Scenario	τ_O^D [$-$, SErf]	α [deg]	δ [deg]	ϵ_D [$-$, SErf]	θ_D [deg]	τ_O^A [$-$, SMrf]	ϵ_A [$-$, SMrf]	θ_A [deg]
Earth-to-Mars	2.3055	62.50	+90.0	1.0170	-147.5	2.9378	0.9925	-45.0
Earth-to-Mercury	1.7929	52.75	-90.0	0.9830	-32.5	0.0306	1.0060	-42.5

(iv) The final state is then propagated backward until it intersects a suitable Poincaré surface of section $Q_A(\theta_A)$, perpendicular to the (x, y)-plane and forming an angle θ_A with the x-axis, after crossing a previous section $P_A(\epsilon_A)$; as per phase (ii), the solar sail control is allowed (i.e. the sail is active) only between these two surfaces. If the trajectory is purely ballistic, then it moves along the stable manifold of the selected LPO, i.e. on $W_{\mathbf{0}}^{\mathbf{O}}(90, \delta_A, -0, \epsilon_A, \theta_A)$, otherwise, if solar radiation pressure is actively exploited, then it moves along the solar sail periodic orbit arrival set $A_{\mathbf{R}}^{\mathbf{O}}(\alpha_A, \delta_A, -\tau_A, \epsilon_A, \theta_A)$.

(v) It is worth underlining that, as the dynamical systems under consideration are different for the two legs of the transfers, a proper operator $\mathcal{T}$ is introduced in order to map states of the arrival dynamical models (Sun–Mars, Sun–Mercury) into the departure one (Sun–Earth). At this phase of the design process, thanks to the mutual independence of the dynamical models, the departure Poincaré section $Q_D(\theta_D)$ and the arrival one $Q_A(\theta_A)$ (after the proper transformation) can be arbitrarily superimposed. After this, on the same SE suitable Poincaré section $Q(\theta)$, the transit point between the solar sail departure set (phase (ii)) and the arrival one (phase (iv)) is searched for, by wisely tuning the introduced design variables.

As for the mapping, for both applicative scenarios, the operator $\mathcal{T}$ is introduced: 1) the states of the arrival model are written in the inertial reference frame with origin at the Sun; 2) the scaled variables are firstly transformed into physical coordinates; 3) the variables are then scaled considering the SE physical constants; 4) the variables are reported into the classic SE rotating frame.

As first guess solutions are being generated at this stage (to be later optimized in more accurate dynamical models), small discontinuities (less than 1.0×10^{-4}) can be tolerated when looking for the patching point.

In summary, the eleven design variables necessary to search for the transfer point and therefore to build first guess solution are (see Tab. 2):

- τ_O^D, the time parameter describing the leaving point on the initial LPO (phase (i));
- α_D, the solar sail cone angle, departure phase (phase (ii));
- δ_D, the solar sail clock angle, departure phase (phase (ii));
- ϵ_D, the location of the section after which solar sail acceleration is exploited (phase (ii));
- θ_D, the Poincaré section angle (phase (ii),(v)) of the departure leg of the transfer;
- τ_O^A, the time parameter describing the insertion point on the final LPO (phase (iii));

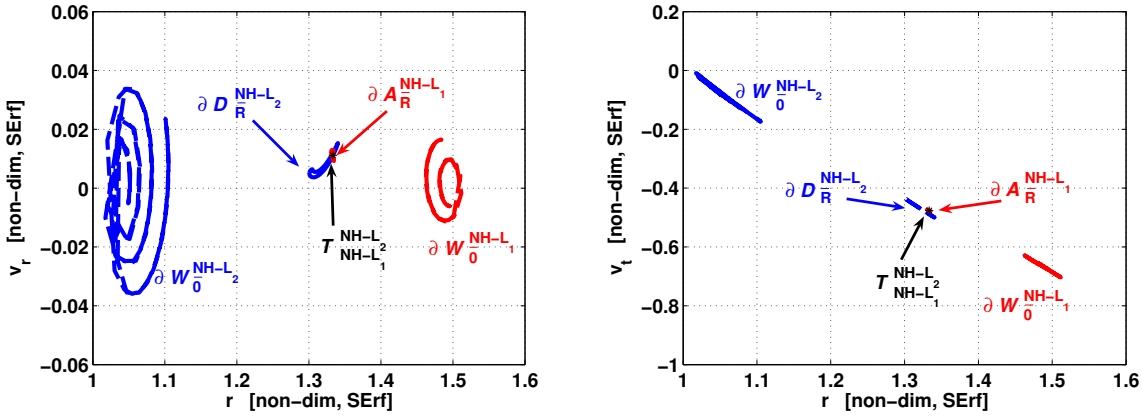

(a) Earth-to-Mars scenario: Poincaré (r, v_r)-section.

(b) Earth-to-Mars scenario: Poincaré (r, v_t)-section.

Figure 8. Phase space on the suitable SE Poincaré sections to design the first guess Earth-to-Mars heteroclinic connection. The blue dashed line stands for the cut of the unstable manifold $\partial W_{\overline{0}}^{\text{NH-L}_2}(90, \delta, 0, \epsilon_D, \theta_D)$, while the blue solid line represents the departure solar sail set $\partial D_{\overline{\text{R}}}^{\text{NH-L}_2}(\alpha, \delta, \tau_D, \epsilon_D, \theta_D)$, both for the initial northern Halo orbit around L_2 of the Sun–Earth system. The red dashed line stands for the cut of the stable manifold $\partial W_{\overline{0}}^{\text{NH-L}_1}(90, \delta, 0, \epsilon_A, \theta_A)$, while the red solid line represents the arrival solar sail set $\partial D_{\overline{\text{R}}}^{\text{NH-L}_1}(\alpha, \delta, -\tau_A, \epsilon_A, \theta_A)$, both for the final northern Halo orbit around L_1 of the Sun–Mars system. Finally, $T_{\text{NH-L}_1}^{\text{NH-L}_2}$ is the transit point.

- α_A, the solar sail cone angle, arrival phase (phase (iv));
- δ_A, the solar sail clock angle, arrival phase (phase (iv));
- ϵ_A, the location of the section after which solar sail acceleration is exploited (phase (iv));
- θ_A, the Poincaré section angle (phase (iv), (v)) of the arrival leg of the transfer;
- β, the solar sail lightness number (used in Eq. 10).

Actually, the set of design variables can be reduced by two when a solar sail constant attitude is considered throughout the complete transfers, i.e. $\alpha_D = \alpha_A = \alpha$, $\delta_D = \delta_A = \delta$. Finally, a constant value of $\beta = 0.050$ is assumed as given by mission requirements.

As described in phase (v), the departure and arrival dynamical models are disjoint, and therefore a transit point in the phase space can be found following the procedure aforementioned. But, being interested in generating initial guesses for interplanetary homoclinic connections, once the geometry of the transfer are defined patching together the two applicable restricted three-body systems, the launch epoch that enables the connection - in the real ephemeris model - is found by means of a systematic search.

Earth-to-Mars Transit Point

The procedure described in the previous section is applied to the Earth-to-Mars mission scenario, in order to design a sample feasible first guess solution, as a function of the corresponding design variables reported in Tab. 2. The departure orbit is a northern Halo orbit around L_2 of the Sun–Earth

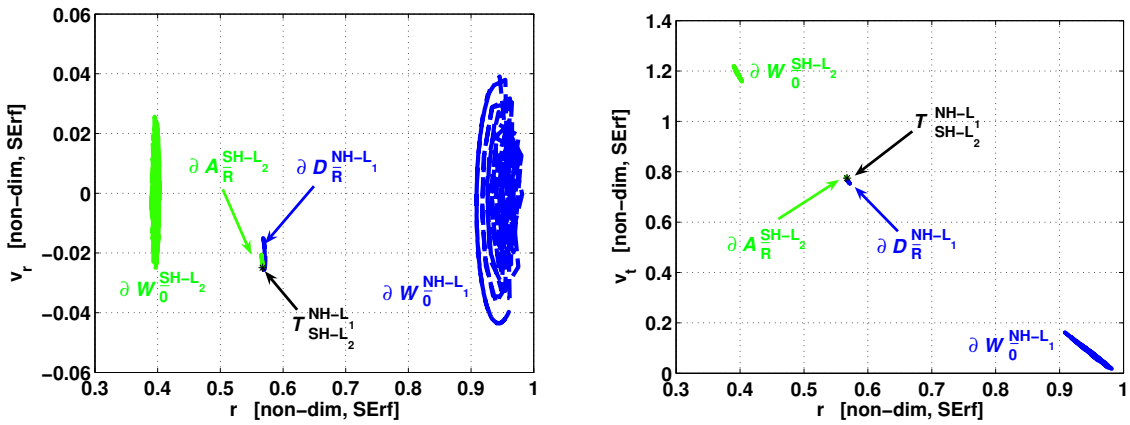

(a) Earth-to-Mercury scenario: Poincaré (r, v_r)-section.

(b) Earth-to-Mercury scenario: Poincaré (r, v_t)-section.

Figure 9. Phase space on the suitable SE Poincaré sections to design the first guess Earth-to-Mercury heteroclinic connection. The blue dashed line stands for the cut of the unstable manifold $\partial W_{\overline{\mathbf{0}}}^{\text{NH-L}_1}(90, \delta, 0, \epsilon_D, \theta_D)$, while the blue solid line represents the departure solar sail set $\partial D_{\overline{\mathbf{R}}}^{\text{NH-L}_1}(\alpha, \delta, \tau_D, \epsilon_D, \theta_D)$, both for the initial northern Halo orbit around L_1 of the Sun–Earth system. The green dashed line stands for the cut of the stable manifold $\partial W_{\overline{\mathbf{0}}}^{\text{NH-L}_2}(90, \delta, 0, \epsilon_A, \theta_A)$, while the green solid line represents the arrival solar sail set $\partial D_{\overline{\mathbf{R}}}^{\text{NH-L}_2}(\alpha, \delta, -\tau_A, \epsilon_A, \theta_A)$, both for the final southern Halo orbit around L_2 of the Sun–Mercury system. Finally, $T_{\text{SH-L}_2}^{\text{NH-L}_1}$ is the transit point.

model, while the arrival one is a northern Halo around L_1 of the Sun–Mars model (see Tab. 1). Basically, the solar sail flies on the exterior SE dedicated solar sail departure set till it is captured on the interior SM dedicated solar sail arrival set.

In Fig. 8 are shown the cuts of the unstable manifold trajectories of the Sun–Earth model, namely $\partial W_{\overline{\mathbf{0}}}^{\text{NH-L}_2}(90, \delta, 0, \epsilon_D, \theta_D)$, and of the solar sail departure dedicated set $\partial D_{\overline{\mathbf{R}}}^{\text{NH-L}_2}(\alpha, \delta, \tau_D, \epsilon_D, \theta_D)$, both for the initial northern Halo orbit around L_2, on the suitable Poincaré sections.

Moreover, on the same suitable Poincaré sections, Fig. 8 presents the cuts of the stable manifold trajectories of the Sun–Mars model $\partial W_{\overline{\mathbf{0}}}^{\text{NH-L}_1}(90, \delta, -0, \epsilon_A, \theta_A)$ and of the solar sail arrival dedicated set $\partial A_{\overline{\mathbf{R}}}^{\text{NH-L}_1}(\alpha, \delta, -\tau_A, \epsilon_A, \theta_A)$, both for the final northern Halo orbit around L_1. The cuts are shown on the (r, v_r)-section and (r, v_t)-section.

For reasonable transfer times, the ballistic manifold structure of the SE and the SM models do not intersect; on the other hand, the Earth-to-Mars heteroclinic first guess solution corresponds to the intersection point

$$T_{\text{NH-L}_1}^{\text{NH-L}_2} \doteq \partial D_{\overline{\mathbf{R}}}^{\text{NH-L}_2}(\alpha, \delta, \tau_D, \epsilon_D, \theta_D) \cap \partial A_{\overline{\mathbf{R}}}^{\text{NH-L}_1}(\alpha, \delta, -\tau_A, \epsilon_A, \theta_A). \tag{20}$$

In the generation process of the first guess solution (to be later optimized in more sophisticated models), small discontinuities (in the out-of-plane components) can be tolerated when looking for the transit point.

Table 3. Transfer performances of the interplanetary (Earth-to-Mars, Earth-to-Mercury) heteroclinic first guess connections.

Applicative Scenario	Departure Date	Arrival Date	Duration [years]	β [–]
Earth-to-Mars	2020/Nov/11	2026/Sep/11	5.8305	0.050
Earth-to-Mercury	2020/Oct/02	2024/Mar/30	3.4894	0.050

Earth-to-Mercury Transit Point

As far as it concerns the Earth-to-Mercury scenario, the same procedure described previously is implemented, in order to design a sample feasible first guess solution, as a function of the corresponding design variables reported in Tab. 2. In this case, the departure orbit is a northern Halo orbit around L_1 of the Sun–Earth model, while the arrival one is a southern Halo around L_2 of the Sun–Mercury model (see Tab. 1). Basically, the solar sail flies on the interior SE dedicated solar sail departure set till it is captured on the exterior SM dedicated solar sail arrival set.

In Fig. 9 are represented the cuts of the unstable manifold trajectories of the Sun–Earth model, $\partial W_{\overline{\mathbf{0}}}^{\text{NH-L}_1}(90, \delta, 0, \epsilon_D, \theta_D)$ and of the solar sail departure dedicated set $\partial D_{\overline{\mathbf{R}}}^{\text{NH-L}_1}(\alpha, \delta, \tau_D, \epsilon_D, \theta_D)$, both for the initial northern Halo orbit around L_1, on the suitable Poincaré sections.

Furthermore, on the same suitable Poincaré sections, in Fig. 9 are shown the cuts of the stable manifold trajectories of the Sun–Mercury model $\partial W_{\overline{\mathbf{0}}}^{\text{SH-L}_2}(90, \delta, -0, \epsilon_A, \theta_A)$ and of the solar sail arrival dedicated set $\partial A_{\overline{\mathbf{R}}}^{\text{SH-L}_2}(\alpha, \delta, -\tau_A, \epsilon_A, \theta_A)$, both for the final southern Halo orbit around L_2. The cuts are shown on the (r, v_r)-section and (r, v_t)-section.

As expected, the pure ballistic manifolds of the SE and the SM models do not intersect; on the other hand, the Earth-to-Mercury heteroclinic first guess solution corresponds to the intersection point

$$T_{\text{SH-L}_2}^{\text{NH-L}_1} \doteq \partial D_{\overline{\mathbf{R}}}^{\text{NH-L}_1}(\alpha, \delta, \tau_D, \epsilon_D, \theta_D) \cap \partial A_{\overline{\mathbf{R}}}^{\text{SH-L}_2}(\alpha, \delta, -\tau_A, \epsilon_A, \theta_A). \tag{21}$$

Again, in the define process of the first guess solution (to be later optimized in more accurate models), small discontinuities (in the out-of-plane components) can be admitted when looking for the transit point.

PRELIMINARY TRANSFER SOLUTIONS

Some preliminary transfer solutions of the Earth-to-Mars and Earth-to-Mercury transfers are presented in Fig. 10 and Fig. 11. Moreover, preliminary transfer performances are reported in Tab. 3.

While Fig. 10(a) and Fig. 10(b) show the transfer in the Sun–Earth synodic reference frame, Fig. 11(a) and Fig. 11(b) use a heliocentric inertial reference frame and also provide information on the solar sail acceleration vector through the use of arrows.

As for the flight time, they are in order of a few years, as expected flying along a manifold-like type of trajectories. For the Earth-to-Mars case, the transfer lasts slightly less then 6 years, while for the Earth-to-Mercury case, it lasts slightly less then 3.5 years.

As the arrows indicate, the performance in terms of acceleration magnitude improves when the solar sail approaches Mercury, i.e. gets closer to the Sun where the photon irradiance and therefore

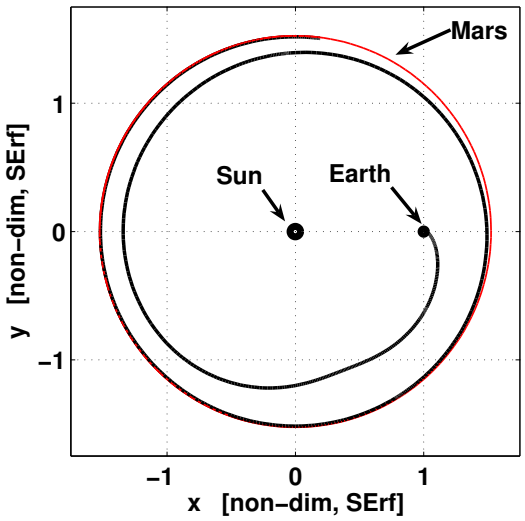

(a) Earth-to-Mars scenario: transfer trajectory in the Sun–Earth rotating frame.

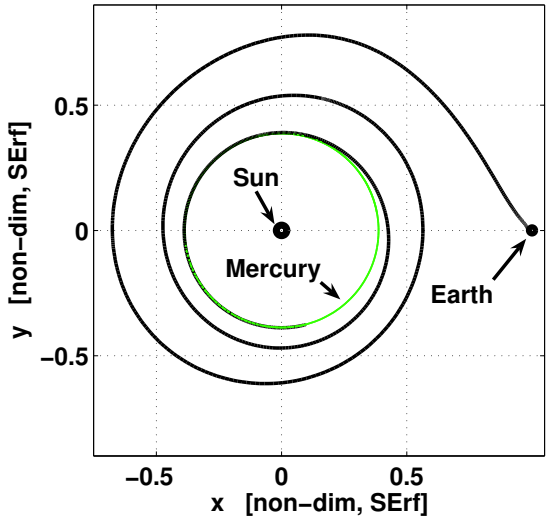

(b) Earth-to-Mercury scenario: transfer trajectory in the Sun–Earth rotating frame.

Figure 10. Applicative scenarios investigated: preliminary transfer trajectories in the Sun–Earth rotating frame.

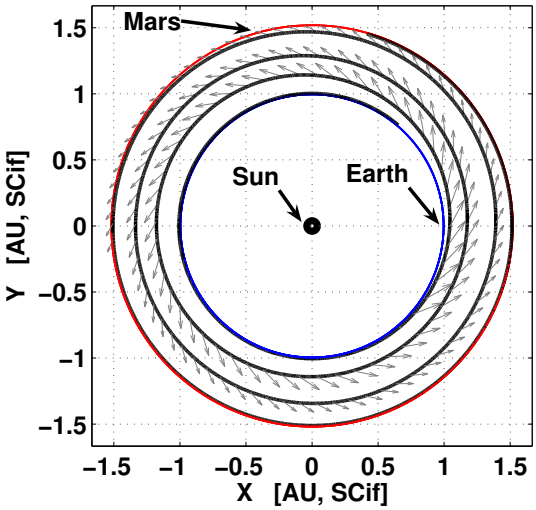

(a) Earth-to-Mars scenario: transfer trajectory in the Sun–centered inertial frame.

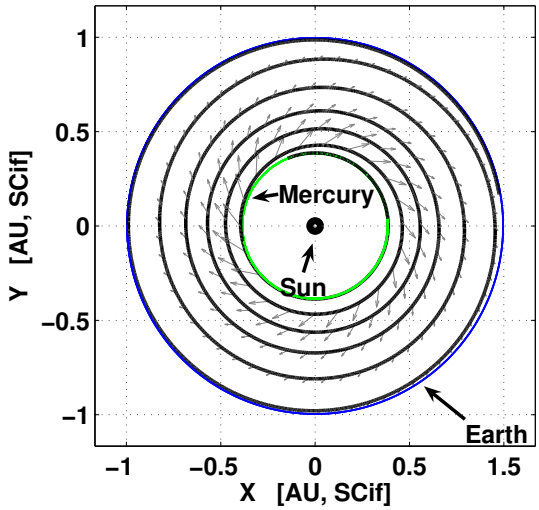

(b) Earth-to-Mercury scenario: transfer trajectory in the Sun–centered inertial frame.

Figure 11. Applicative scenarios investigated: preliminary transfer trajectories in the Sun–Centered inertial frame.

solar sail acceleration is larger than at Earth distance. On the other hand, the acceleration magnitude decreases during the Earth-to-Mars transfer case, as the spacecraft moves away from the Sun (see also Fig. 12).

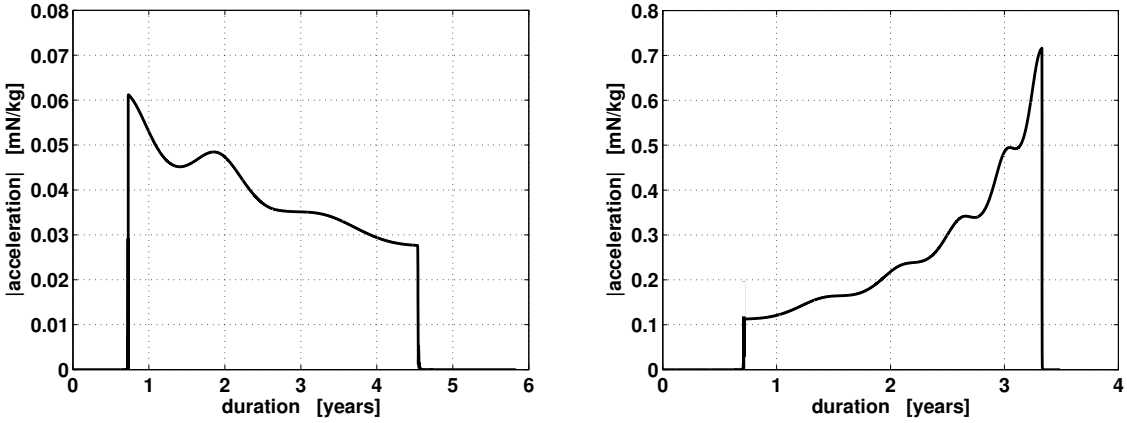

(a) Earth-to-Mars scenario: control acceleration profile.

(b) Earth-to-Mercury scenario: control acceleration profile.

Figure 12. Applicative scenarios investigated: solar sail acceleration profiles.

Further Investigation

The solar sail interplanetary heteroclinic fist guesses investigated in this work are the initial seeds optimized in the paper by Heiligers.[20] The fist guess connections discussed previously reveal to be sub-optimal as there could be minor discontinuities in position and velocities at the transit points between the two three-body systems. In summary, the discontinuities can be solved by transferring the first-guess trajectories to a direct pseudospectral method, which discretises the time interval into a finite number of collocation points and uses Legendre or Chebyshev polynomials to approximate and interpolate the time dependent variables at the collocation points. This way, the infinite dimensional optimal control problem is transformed into a finite dimension non-linear programming (NLP) problem. Pseudospectral methods have become increasingly of interest for solving optimal control problem because the characteristics of the orthogonal polynomials are very well suited to the mathematical operations required to solve the optimal control problem: functions can be very accurately approximated, derivatives of the state functions at the nodes are computed by matrix multiplication only and any integral associated with the problem is approximated using well-known Gauss quadrature rules. This, together with the fact that pseudospectral methods have a rapid rate of convergence (i.e. convergence to a very accurate solution with few number of nodes), is the reason for using pseudospectral methods in paper Ref. 20, where a particular implementation of a direct pseudospectral method is chosen, i.e. PSOPT.[21] PSOPT is an open source tool developed by Victor M. Becerra of the University of Reading and is written in C++ and is interfaced to IPOPT (Interior Point OPTimizer)[22] to solve the NLP problem.

CONCLUSIONS

In this paper, the first-guess generation process - based on a few design variables - of solar sail trajectories for two different applicative scenarios was investigated. In detail, LPOs belonging to the Sun–Earth system are linked to LPOs of the Sun–Mars and the Sun–Mercury one, respectively. Special *dedicated sets* were introduced to exploit the combined use of solar radiation pressure with invariant manifold trajectories. This approach enabled a radically new class of missions; the key

idea was to replace invariant manifolds with *solar sail sets*, and to manipulate the latter in the same way the manifolds are used to design space transfers. By including a solar sail acceleration and fixing the attitude of the solar sail with respect to the Sun-sail line, intersections between restricted three-body models were found on suitable Poincaré surface of sections. Alongside the exploitation of the n-body problems' intrinsic dynamics, the propellant-free feature of solar sails was used in order to generate efficient trajectories. The preliminary propellant-free transfer trajectories revealed to be promising from the optimization perspective, as demonstrated in paper Ref. 20, where different solar sail attitude policies are also implemented.

ACKNOWLEDGEMENT

This research was performed in the framework of the project supported by the European Research Council Advanced Investigator Grant – 227571: VISIONSPACE, Orbital Dynamics at Extremes of Spacecraft Length-Scale.

REFERENCES

[1] Y. Tsuda, O. Mori, R. Funase, H. Sawada, T. Yamamoto, T. Saiki, T. Endo, and J. Kawaguchi, "Flight Status of IKAROS Deep Space Solar Sail Demonstrator," *Acta Astronautica*, Vol. 69, 2011, pp. 833–840.

[2] L. Johnson, M. Whorton, A. Heaton, R. Pinson, G. Laue, and C. Adams, "A Solar Sail Demonstration Mission," *Acta Astronautica*, Vol. 68, 2011, pp. 571–575.

[3] C. McInnes and J. Simmons, "Solar Sail Halo Orbits. Part I - Heliocentric Case," *Journal of Spacecraft and Rockets*, Vol. 29, 1992, pp. 466–471.

[4] H. Baoyin and C. McInnes, "Solar Sail Halo Orbits at the Sun-Earth Artificial L1-Point," *Celestial Mechanics and Dynamical Astronomy*, Vol. 94, 2006, pp. 155–171.

[5] J. Heiligers and C. McInnes, "Agile Solar Sailing in Three-body Problem: Motion Between Artificial Equilibrium Points," 64th *International Astronautical Congress, Beijing, China, 23–27 September*, 2013.

[6] P. Pergola, K. Geurts, C. Casaregola, and M. Andrenucci, "Earth–Mars Halo to Halo Low Thrust Manifold Transfers," *Celestial Mechanics and Dynamical Astronomy*, Vol. 105, 2009, pp. 19–32.

[7] F. Topputo, M. Vasile, and F. Bernelli-Zazzera, "Low Energy Interplanetary Transfers Exploiting Invariant Manifolds of the Restricted Three-Body Problem," *Journal of the Astronautical Sciences*, Vol. 53, 2005, pp. 353–372.

[8] G. Mingotti, F. Topputo, and F. Bernelli-Zazzera, "Earth-Mars Transfers with Ballistic Escape and Low-Thrust Capture," *Celestial Mechanics and Dynamical Astronomy*, Vol. 110, 2011, pp. 169–188.

[9] V. Szebehely, *Theory of Orbits: The Restricted Problem of Three Bodies*. Academic Press Inc., New York, 1967.

[10] C. Conley, "Low Energy Transit Orbits in the Restricted Three-Body Problem," *SIAM Journal on Applied Mathematics*, Vol. 16, 1968, pp. 732–746.

[11] J. Llibre, R. Martínez, and C. Simó, "Transversality of the Invariant Manifolds Associated to the Lyapunov Family of Periodic Orbits Near L_2 in the Restricted Three-Body Problem," *Journal of Differential Equations*, Vol. 58, 1985, pp. 104–156.

[12] G. Gómez, A. Jorba, J. Masdemont, and C. Simó, "Study of the Transfer from the Earth to a Halo Orbit around the Equilibrium Point L1," *Celestial Mechanics and Dynamical Astronomy*, Vol. 56, 1993, pp. 239–259.

[13] A. Jorba and J. Masdemont, "Dynamics in the Center Manifold of the Collinear Points of the Restricted Three Body Problem," *Physica D*, Vol. 132, 1999, pp. 189–213.

[14] D. Richardson, "Halo-orbit Formulation for the ISEE-3 Mission," *American Institute of Aeronautics and Astronautics Conference*, 1979.

[15] D. Richardson, "Analytic construction of periodic orbits about the collinear points," *Celestial Mechanics and Dynamical Astronomy*, Vol. 22, No. 3, 1980, pp. 241–253.

[16] W. Koon, M. Lo, J. Marsden, and S. Ross, "Heteroclinic Connections between Periodic Orbits and Resonance Transitions in Celestial Mechanics," *Chaos*, Vol. 10, 2000, pp. 427–469.

[17] S. Wiggins, *Introduction to Applied Nonlinear Dynamical Systems and Chaos*. Springer Verlag, 2003.

[18] M. Ozimek and K. Howell, "Low-Thrust Transfers in the Earth–Moon System Including Applications to Libration Point Orbits," *Journal of Guidance, Control, and Dynamics*, Vol. 33, No. 2, 2010, pp. 533–549.

[19] C. McInnes, *Solar Sailing: Technology, Dynamics and Mission Applications*. Springer-Praxis Books in Astronautical Engineering, Springer-Verlag, Berlin, 1999.

[20] J. Heiligers, G. Mingotti, and C. McInnes, "Optimisation of Solar Sail Interplanetary Heteroclinic Connections," 2nd *IAA Conference on Dynamics and Control of Space Systems - DyCoSS' 2014, Rome, Italy, 24–26 March*, 2014.

[21] V. Becerra, "Solving Complex Optimal Control Problems at No Cost with PSOPT," *Computer-Aided Control System Design (CACSD), 2010 IEEE International Symposium on*, 2010, pp. 1391–1396.

[22] A. Wächter and L. Biegler, "On The Implementation of an Interior-Point Filter Line-Search Algorithm for Large-Scale Nonlinear Programming," *Mathematical programming*, Vol. 106, No. 1, 2006, pp. 25–57.